

Computed Rotational Collision Rate Coefficients for Recently Detected Anionic Cyanopolyynes

L. GONZÁLEZ-SÁNCHEZ,¹ A. VESELINOVA,¹ A. MARTÍN SANTA DARÍA,¹ E. YURTSEVER,² R. BISWAS,³ K. GIRI,⁴
N. SATHYAMURTHY,⁵ U. LOURDERAJ,³ R. WESTER,⁶ AND F. A. GIANTURCO⁶

¹*Departamento de Química Física, University of Salamanca, Plaza de los Caídos sn, 37008, Salamanca, Spain*

²*Department of Chemistry, Koc University Rumelifeneriyolu, Sariyer TR 34450, Istanbul, Turkey*

³*School of Chemical Sciences, National Institute of Science Education and Research (NISER) Bhubaneswar*

⁴*Department of Computational Sciences, Central University of Punjab, Bathinda, Punjab 151401, India*

⁵*Indian Institute of Science Education and Research Mohali, SAS Nagar, Punjab 140306, India*

⁶*Institut für Ionenphysik und Angewandte Physik, Universität Innsbruck Technikerstr. 25 A-6020, Innsbruck, Austria*

(Dated: October 31, 2023)

ABSTRACT

We report new results from quantum calculations of energy-transfer processes taking place in interstellar environments and involving two newly observed molecular species: C_5N^- and C_7N^- in collision with He atoms and the p- H_2 molecules. These species are part of the anionic molecular chains labeled as cyanopolyynes which have been observed over the years in molecule-rich Circumstellar Envelopes (CSEs) and in molecular clouds. In the present work, we first carry out new *ab initio* calculations for the C_7N^- interaction potential with He atom and then obtain state-to-state rotationally inelastic cross sections and rate coefficients involving the same transitions which have been observed experimentally by emission in the interstellar medium (ISM) from both of these linear species. For the C_5N^- /He system we extend the calculations already published in our earlier work (see reference below) to compare more directly the two molecular anions. We extend further the quantum calculations by also computing in this work collision rate coefficients for the hydrogen molecule interacting with C_5N^- , using our previously computed interaction potential. Additionally, we obtain the same rate coefficients for the C_7N^- / H_2 system by using a scaling procedure that makes use of the new C_7N^- /He rate coefficients, as discussed in detail in the present paper. Their significance in affecting internal state populations in ISM environments where the title anions have been found is analyzed by using the concept of critical density indicators. Finally, similarities and differences between such species and the comparative efficiency of their collision rate coefficients are discussed. These new calculations suggest that, at least for the case of these longer chains, the rotational populations could reach local thermal equilibrium (LTE) conditions within their observational environments.

1. INTRODUCTION

The study of the molecular complexity of the interstellar medium (ISM) provides us with fundamental information on the chemical storage of species and on the energy available for the formation of stars and planets. It also gives us useful indication about the chemical inventory that the primitive Earth might have inherited and about the formation paths of many of the species increasingly discovered by direct observations.

In recent years, several linear C-bearing and (C,N)-bearing chains of molecular anions have been detected at various sites in the circumstellar envelopes (CSE)

and in molecular clouds. Specifically: CN^- Agúndez, M. et al. (2010), C_3N^- Thaddeus et al. (2008), C_5N^- Cernicharo et al. (2008); Cernicharo, J. et al. (2020), C_4H^- Cernicharo, J. et al. (2007); Agúndez, M. et al. (2008), C_6H^- McCarthy et al. (2006), and C_8H^- Brünken et al. (2007); Remijan et al. (2007). Those reported so far constitute different terms of the general linear chains associated with the polyynes and cyanopolyynes species. Interestingly, very recently two additional (C,N)-bearing chains have been detected. They involve the two longest sequences of the linear-chain series observed so far : $C_{10}H^-$ Remijan et al. (2023) and C_7N^- Cernicharo et al. (2023).

The chemistry of formation of the cyanopolyne chains has also been the object of several studies and

speculations (e.g. see: [Khamesian et al. \(2016\)](#); [Cernicharo, J. et al. \(2020\)](#)). The possible formation of anions from the neutral radical via a Radiative Electron Attachment (REA) process has been considered in some detail (as quoted in: [Jerosimić et al. \(2018\)](#)) while a more direct chemical route by reaction of the HC_5N with H^- has also been put forward by our group [Satta et al. \(2015\)](#). Another possible mechanism of formation could be the reaction between N atom and C_n^- , as discussed in: [Cernicharo, J. et al. \(2020\)](#). For the present case of the C_5N^- our calculated rates were found to be large enough to be relevant within the chemical evolution producing these anions. As also discussed by [Cernicharo, J. et al. \(2020\)](#) the much larger rate constant for the REA formation path expected for C_5N compared to C_3N is the main reason why C_5N^- has been estimated to be much more abundant with respect to the neutral than C_3N^- (the abundance ratios of the $\text{C}_n\text{N}^- / \text{C}_n\text{N}$ are ~ 140 and 2.3 for $n = 3$ and $n = 5$, respectively, in the Taurus molecular cloud 1 (TMC-1)). For the case of the longer chain of the C_7N^- anion its abundance ratio with the next smaller chain discussed in the present work, the C_5N^- anion, was found in the molecular cloud TMC-1 to be around 5 in [Cernicharo et al. \(2023\)](#). On the other hand, the same $\text{C}_5\text{N}^- / \text{C}_7\text{N}^-$ ratio in the IRC-10216 was indicated in the same study to be around 2.4, i.e. not very different from the situation in the TMC-1 environment. In the final analysis, however, the various options put forward by the current literature about the chemical paths to the formation of the cyanopolynes have not yet coalesced into a unique proof of the chemical mechanism for the title anions or for their smaller partners in the series.

Astrophysical observation of these molecular anions relies heavily on the spectroscopic investigation of their properties in the laboratory and on matching sighted lines with those observed in the earthly experiments. Additionally, to carry out astrophysical modeling of molecular population evolution from their distributions over a variety of internal states, important indicators are provided by the rate coefficients for the probability of rotational state-changes in molecular species induced by their interaction with He and H_2 , both partners being present in substantial amounts in the observational environments of these anions. The collision-induced occurrence of non-LTE (Local Thermal Equilibrium) population distribution for rotational states in molecular partners could, in fact, be a significant path to produce radiative emissions from different excited spectral lines in the observational microwave regions. Measurement of these rate coefficients in the laboratory is still challenging, while available quantum methods can be

used to model such processes and then enter their results within networks of the kinetics of the underlying chemistry or of the internal-state populations in different environments. For example, [Botschwina and Oswald](#) [Botschwina & Oswald \(2008\)](#) had computationally determined the structural characteristics of some of these species to help observational sighting in the ISM or in the laboratory of specific emission lines

In the present work we focus more specifically on the collision-induced rotational state-changing processes associated with the observed emission lines involving the $\text{C}_5\text{N}^- / \text{C}_7\text{N}^-$ anions, those discussed in the recent publications of ([Cernicharo, J. et al. 2020](#); [Cernicharo et al. 2023](#)) respectively. We thus compute the inelastic rate coefficients activated by interaction with He atoms and with p- H_2 molecules over the same range of transitions, and further calculate the Einstein A-coefficients of spontaneous emissions between the same rotational levels of these molecular anions. We then analyze the behaviour of the critical densities over the temperature range in the molecular clouds where the observations were made and discuss the consequences that such indicators suggest for the local distributions among rotational states in both molecules. The state-changing collision rate coefficients are obtained using exact quantum computations in the cases of both the C_5N^- and the C_7N^- anions in collision with the He atoms. For the H_2 collision partner exact calculations are carried out for the $\text{C}_5\text{N}^- / \text{H}_2$ system, while a scaling procedure is implemented for the H_2 collision rates with the C_7N^- longer anion, making use of the new rates from the $\text{C}_7\text{N}^- / \text{He}$ system and from the $\text{C}_5\text{N}^- / \text{H}_2 / \text{He}$ systems, as discussed in detail later in this paper. The details of the calculations and the analysis of the obtained results will be presented in the following Sections, while our conclusions will be given in the last Section.

2. THE AB INITIO COMPUTED INTERACTION POTENTIAL

The calculations of the new Potential Energy Surface (PES) for the $\text{C}_7\text{N}^- / \text{He}$ system were carried out using the GAUSSIAN09 set of codes as in [Frisch et al. \(2009\)](#) with the UCCSD(T) approach based on initial UHF orbital expansion using the aug-cc-pVTZ for the carbon and nitrogen atoms, while for the He atomic partner the more extended basis set was of QZ-Vpp quality. For further details on the atomic basis we have employed see: [Dunning Jr \(1989\)](#) and [Weigend & Ahlrichs \(2005\)](#). The usual BSSE correction was applied: [Frisch et al. \(2009\)](#), [Deega & Knowles \(1994\)](#), [Woon & Dunning Jr \(1994\)](#). No convergence problems were encountered in the calculations. In all the *ab initio* calculations we used an an-

gular grid of 5° intervals. The optimized bond distances in the C_5N^- partner were taken from our previous calculations described in our earlier publication [Biswas, R. et al. \(2023\)](#) where all the details of this anion's interaction with both He and H_2 were reported. Hence, we shall not be repeating this information in this Section, where we shall discuss instead the new calculations we have carried out for the longer anionic chain.

In the case of the C_7N^- partner, the optimized bond distances were obtained from such new calculations. Hence, if one takes the carbon atom at the extreme left as the origin of the x -coordinate, then the C_1 - C_2 distance was (all values in Å): 1.2648, the C_2 - C_3 distance: 1.4062; the C_3 - C_4 bond: 1.2413; the C_4 - C_5 bond: 1.2784; the C_5 - C_6 bond: 1.2318; the C_6 - C_7 bond: 1.3643; the N- C_7 distance: 1.1707 for a total length of the linear cyanopolyynes of 8.9575 and the c.o.m. (center-of-mass) location at 4.6002. The resulting interaction with the He atom was described via the distance R from the c.o.m. and the polar angle θ , both being the usual 2D Jacobi coordinates which describe the present PES.

The radial range of the raw points for the variable R was taken from initial values of around 6.2 Å depending on the particular angular orientation, and extended out to 20.0 Å. Radial intervals between 0.1 to 1.0 Å were used depending on the distance and angle regions from the c.o.m. A variable number of radial values for each angular orientation were obtained as raw points, for a total range of 37 angular values. Note that the long, linear structure of the anionic species, and hence the location of the center-of-mass at the large distance mentioned earlier, are responsible for the interaction to become highly repulsive at fairly large distances for the atomic partner's approach to the c.o.m. We shall further show below that the actual radial range of the fitted potentials came closer to the c.o.m positions for some of the angles needed in the scattering calculations. It is important to note at this point that the *ab initio* computed points are not symmetrically distributed along the distance coordinate due to the large anisotropy of the system, depending on the entrance angle of the He atom. This specific feature of the forces at play will be further discussed below.

This lack of points at short distances was therefore improved and completed by extrapolating with an exponential function for every angle up to 2 Å with respect to the c.o.m. In order to generate a uniformly regular grid of points, spline functions were used on the *ab initio* and on the extrapolated data sets to produce a total of 82 distance (R) points along the 37 angles (θ), summing up to a total of 3034 points which were further fitted

to generate the final PES. The intrinsic problem of having 'ghost points' at very short distances, even without them having physical sense because of their being inside the anionic atoms' chain itself, is their extremely large energy values which accumulate over short radial intervals. Such huge values cause mathematical instabilities when trying to fit them via an analytical function. To overcome this problem, we scaled the points by applying the simple procedure implemented by [Faure et al. \(2011\)](#) and already used in similar systems [Khadri et al. \(2020\)](#); [Sahnoun et al. \(2018\)](#); [Massó & Wiesenfeld \(2014\)](#). It has the advantage that one can now reproduce the original *ab initio* points in the lower energy range of the PES (the most relevant range for the scattering calculations) while one only scales the higher energy values that would not be sampled during the scattering events. Thus, one can write the following sequence,

$$\begin{aligned} V_s &= V_a && \text{for } V_a \leq V_{T1} \\ V_s &= V_{T1} + (V_{T2} - V_{T1}) S\left(\frac{V_a - V_{T1}}{V_{T2} - V_{T1}}\right) && \text{for } V_{T1} < V_a \leq V_{T2} \\ V_s &= V_{T1} + \frac{2}{\pi}(V_{T2} - V_{T1}) && \text{for } V_a > V_{T2} \end{aligned} \quad (1)$$

where V_s is the scaled potential, V_a is the *ab initio* energy and V_{T1} and V_{T2} refer to two threshold energy values, which for this particular case are 2000 cm^{-1} and 10000 cm^{-1} , respectively. The switching function is given by the S function defined as

$$S(x) = \frac{2}{\pi} \sin \left[\frac{\pi}{2} \sin \left(\frac{\pi}{2} x \right) \right], \quad (2)$$

and it guarantees the proper transition between the three different scaling windows.

In the standard procedures employed for solving the Coupled-Channel (CC) scattering equations, it is usually convenient, as discussed below, to expand the interaction potential $V(R, \theta)$ into orthogonal angular functions ([Arthurs & Dalgarno 1960](#); [Secret 1979](#); [Kouri & Hoffman 1997](#); [Gianturco 1979](#)). Hence, for a more direct, and quantitative evaluation of the spatial anisotropy around the C_5N^- and the C_7N^- linear anions it is useful to represent the raw, 2D grid of points from the *ab initio* calculations in terms of the familiar Legendre polynomials in their standard (R, θ) form. In the case of the new calculations discussed above, using the 3034 'scaled points' we were able to expand the PES via the usual orthogonal Legendre polynomials for the θ angle:

$$V_{\text{FIT}} = V(R, \theta) = \sum_{\lambda=0}^{\lambda_{\text{max}}} V_{\lambda}(R) P_{\lambda}(\cos \theta) \quad (3)$$

The fitted potential is restricted to a finite range of R values and therefore an extrapolation to an asymptotic form is needed to describe the long-range interaction forces. The analytical form used for the long-range is

$$V_{\text{LR}}(\theta) = -\frac{\alpha_0}{2R^4} + \frac{2\alpha_0\mu}{R^5} \cos \theta, \quad (4)$$

where $\alpha_0 = 1.41 a_0^3$, is the polarizability of the He atom and $\mu = 7.5D$, from [Cernicharo et al. \(2023\)](#), is the rigid rotor dipole moment of the C_7N^- anionic partner.

To ensure the smooth transition between the V_{FIT} fitted PES (Eq. 3) and the V_{LR} long-range term (Eq. 4) in the construction of the V_{f} final PES, the switching procedure which was already used for $\text{C}_5\text{N}^-/\text{He}$ [Biswas, R. et al. \(2023\)](#) has also been implemented for the longer chain anion:

$$V_{\text{f}} = f_s V_{\text{FIT}} + (1 - f_s) V_{\text{LR}} \quad (5)$$

where the switching function is

$$f_s(R) = \frac{1}{e^{\frac{(R-R_0)}{\Delta R}} + 1}, \quad (6)$$

with $R_0 = 18.5$ and $\Delta R = 1.2 \text{ \AA}$.

A pictorial view of the spatial shape of the interaction forces for $\text{C}_7\text{N}^-/\text{He}$ is reported in Figure 1, where the energy isolines are depicted around the linear, rod-like structure of the anionic partner.

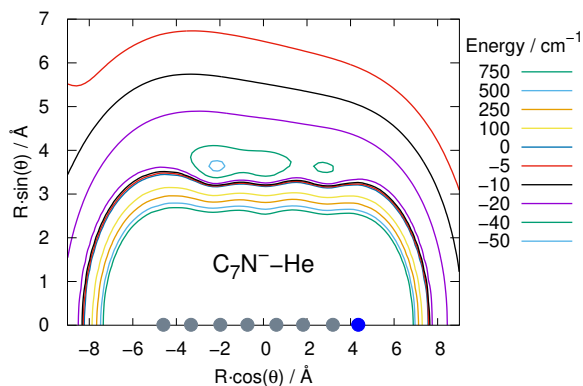


Figure 1. Pictorial representation of the spatial features of the interaction between the C_7N^- partner and the He atom. The first C atom is on the left while the end N atom is on the right. See main text for further details.

It is interesting to note from the structure of the isolines that the interaction becomes, at all angles, very repulsive at rather large distances from the c.o.m., a

difficult feature to represent, as we have already discussed earlier, and which reflects the unusually long, linear structure of this anionic target. We further see that the attractive regions of its interaction with a neutral He atom are located within a fairly localized valley corresponding to a T-shaped configuration of the van der Waals complex. Finally, the ‘oscillations’ shown by the isolines, as one comes closer to the chain of carbon atoms, indicate the detailed changes of the interaction forces with the approaching He partner as one moves from the carbon atoms to the bonding sections along the molecular chain.

The multipolar expansion was carried out to λ values up to $\lambda = 93$, to ensure numerical convergence, employing the procedure discussed more extensively earlier in this Section, where we explain how a larger number of raw points were obtained by adding to the initial selection. The actual features of the multipolar coefficients for the C_5N^- partner with the He projectile were discussed in detail in our earlier work reported by ref [Biswas, R. et al. \(2023\)](#), hence we shall not be repeating it in the present paper. We only report in Figure 2 a comparison between the lower six coefficients newly obtained for the longer molecular anion, the C_7N^- , and those we had found earlier for the C_5N^- anion, to indicate the relative strength of the angular coupling that will be active for the various radial regions of their interactions with the neutral He atoms. The multipolar coefficients reported in that Figure are usually found to be the more effective during the quantum dynamics couplings of target rotational levels, as further discussed in the next Section.

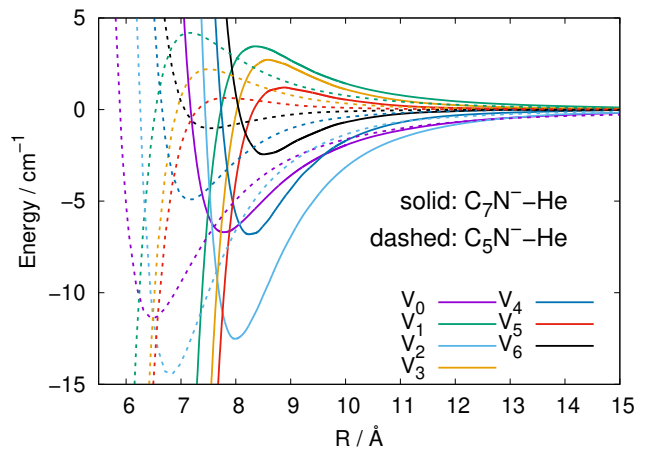


Figure 2. A comparison of the lower radial multipolar coefficients for the interaction potential energy surfaces between the C_5N^- and the C_7N^- anions and the He atom. See main text for further comments.

As it is to be expected, the interactions with $\lambda=0$ exhibit the largest well depths for their attractive regions, while the next strong interactions come from the $\lambda=1$ and 2 coefficients for both partners. These coefficients also present marked well depths. The significance of having these radial coefficients providing large anisotropic couplings will be discussed further in the next Section.

The computed rotational constants for the two anions, treated at the level of spherical, rigid rotors in $^1\Sigma$ states (see further discussion below) were both found to be fairly small, as is to be expected for such long molecular chains: the B_e value is 0.046292 cm^{-1} for the C_5N^- molecule and 0.01942 cm^{-1} for the C_7N^- anion as discussed in Cernicharo, J. et al. (2020) and in Cernicharo et al. (2023). For a comparison between the two rotational energy ladders which involve the range of states which have been experimentally detected in Cernicharo, J. et al. (2020) and in Cernicharo et al. (2023), we report in Figure 3 the relative positioning of these states for the two molecules. We clearly see there that the relevant levels cover in each case about 20 or so cm^{-1} and that many more states are available in that range for the longer anion on the right of the figure. Such features indeed suggest the occurrence of strong coupling between the closely spaced levels during the dynamical steps, as we shall further discuss below.

As a result of the relatively large number of states which can be available over rather small ranges of collision energies, we can argue that at the temperatures reported by the experimental observations of either anion and further discussed below, the reaching of an LTE condition could involve states up to about $j_{max} = 50$ or $= 60$ to be contributing to rotational state populations up to 50 K. This structural feature will further be discussed later when we shall examine the results from collision and radiative processes involving both molecular anions.

3. ROTATIONALLY INELASTIC QUANTUM DYNAMICS

Since in our present study no chemical modifications occur during the collision events, the total scattering wave function can be expanded in terms of asymptotic target rotational eigenfunctions (taken to be spherical harmonics) whose eigenvalues are given by $B_e j(j+1)$ where B_e is the first rotational constant mentioned earlier for the present systems (Arthurs & Dalgarno 1960; Secrest 1979; Kouri & Hoffman 1997; Gianturco 1979). The channel components for the CC formulation are therefore expanded into products of total angular momentum eigenfunctions and of radial functions (Arthurs

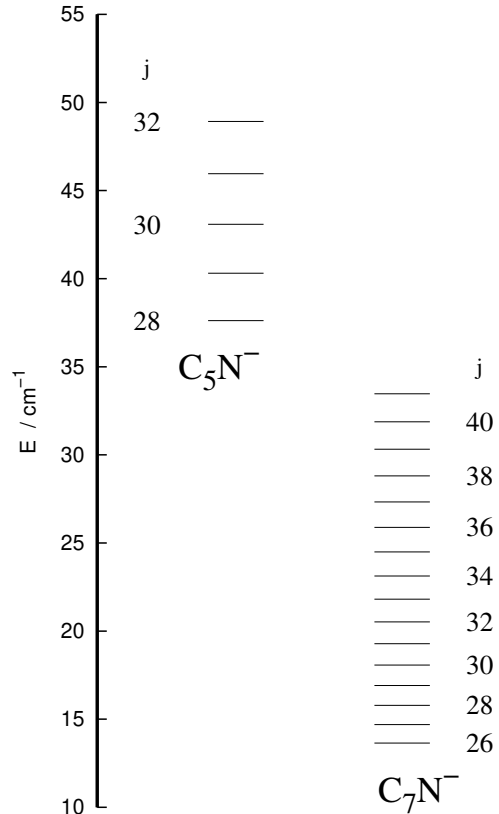


Figure 3. Energy ladders of the rotational levels of the two molecular anions of this study within the range of the observed transitions in the ISM. See main text for further comments

& Dalgarno 1960). The latter are in turn the elements of the solutions matrix which appear in the familiar set of coupled, second order homogeneous differential equations:

$$\left(\frac{d^2}{dR^2} + \mathbf{K}^2 - \mathbf{V} - \frac{\mathbf{l}^2}{R^2} \right) \Psi = 0 \quad (7)$$

where $[\mathbf{K}]_{ij} = \delta_{i,j} 2\mu(E - \epsilon_i)$ are the matrix elements of the diagonal matrix of the asymptotic (squared) wavevectors and $[\mathbf{l}]_{ij} = \delta_{i,j} l_i(l_i + 1)$ is the matrix representation of the square of the orbital angular momentum operator. This matrix is block-diagonal with two sub-blocks that contain only even values of $(l' + j')$ or only odd values of $(l' + j')$.

The scattering observables are thus obtained in the asymptotic region where the Log-Derivative matrix has a known form in terms of free-particle solutions and unknown mixing coefficients. For example, in the asymptotic region the solution matrix can be written in the form:

$$\Psi = \mathbf{J}(R) - \mathbf{N}(R)\mathbf{K} \quad (8)$$

where $\mathbf{J}(R)$ and $\mathbf{N}(R)$ are matrices of Riccati-Bessel and Riccati-Neumann functions. Therefore, at the end of the propagation one uses the Log-Derivative matrix to obtain the \mathbf{K} matrix by solving the following linear system:

$$(\mathbf{N}' - \mathbf{Y}\mathbf{N}) = \mathbf{J}' - \mathbf{Y}\mathbf{J} \quad (9)$$

and from the \mathbf{K} matrix the S-matrix is easily obtained and from it the state-to-state cross sections. We have already published an algorithm that modifies the variable phase approach to solve that problem, specifically addressing the latter point and we defer the interested reader to these references for further details (López-Durán et al. 2008; Martinazzo et al. 2003). In the present calculations we first generated the necessary state-to-state rotationally inelastic cross sections and, once these quantities were known, the required rotationally inelastic rate coefficients $k_{j \rightarrow j'}(T)$ were evaluated as the convolution of these cross sections $\sigma_{j \rightarrow j'}$ over a Boltzmann distribution of the relative translational energy values between partners (E_{trans}):

$$k_{j \rightarrow j'}(T) = \left(\frac{8}{\pi \mu k_B^3 T^3} \right)^{1/2} \times \int_0^\infty E_{\text{trans}} \sigma_{j \rightarrow j'}(E_{\text{trans}}) e^{-E_{\text{trans}}/k_B T} dE_{\text{trans}} \quad (10)$$

The reduced masses for the $\text{C}_5\text{N}^-/\text{He}$ and $\text{C}_7\text{N}^-/\text{He}$ systems were (in units of amu): 3.797372 and 3.8455, respectively. The individual rate coefficients were obtained at intervals of 1 K, starting from 20 K and going up to 50 K. The new scattering calculations for the larger C_7N^- anion were carried out using the MOLSCAT suite of codes (Hutson & Sueur 2019a,b).

Briefly, We have included 87 rotational states for the $\text{C}_5\text{N}^-/\text{He}$ system and two rotational states for H_2 for our calculations on the $\text{C}_5\text{N}^-/\text{H}_2$ system. The maximum value of J_{TOT} was 200, depending on the energy. The convergence checks of the results indicated an accuracy of the cross sections around 2-3%. The spacing of the energy points (in cm^{-1}) for the cross section calculations varied from 0.1 up to 15.0, to 5.0 up to 180.0 and then to 25.0 up to the largest energies of about 350.0 cm^{-1} . In the case of the $\text{C}_7\text{N}^-/\text{He}$ system we found that, for the studied transitions, to include rotational states up to $j_{max}=60$ were enough, and the maximum value of J_{TOT} was 180, depending on the energy. Regarding the energy points, we did not use a regular grid. To ensure the convergence of the rate constants to the same values mentioned before in the same interval of temperatures, we have considered, for all initial states,

collision energies from 0.001 to 2.5 cm^{-1} and total energies from 10 to 300 cm^{-1} .

We should further note here that at the highest collision energies considered, i.e. above 140 cm^{-1} , we have switched from the full Coupled Channel (CC) approach to the reduction scheme of the Coupled States (CS) approach as described in (Hutson & Sueur 2019a,b). Furthermore, at some of the selected high energy values we additionally run calculations at the CC level for comparison and found that the actual cross sections remained within 2-3% of the CS values.

4. EINSTEIN COEFFICIENTS FOR RADIATIVE EMISSION

Another important process for characterizing the internal state distribution of the anions is their interaction with the surrounding radiative field, also known as black-body radiation. The total emission (em) transition rates from an excited state X can be written as sum of stimulated (sti) and spontaneous (spo) emission rate coefficients, as discussed in detail in, e.g.: Brown & Carrington (2003) and as defined below:

$$X_{k \rightarrow i}^{em} = X_{k \rightarrow i}^{sti} + X_{k \rightarrow i}^{spo} = A_{k \rightarrow i}(1 + \eta_\gamma(\nu, T)) \quad (11)$$

where $A_{k \rightarrow i}$ is the Einstein coefficient for spontaneous emission and $\eta_\gamma(\nu, T) = (e^{(h\nu/k_B T)} - 1)^{-1}$ is the Bose-Einstein photon occupation number for the stimulated processes. In the present study the most important role is played by the spontaneous emission step, since in the fairly low photon densities of the regions of the diffuse molecular clouds, which we are considering relevant here, make the stimulated processes less likely to occur.

The Einstein coefficient for dipole transitions is given as

$$A_{k \rightarrow i} = \frac{2}{3} \frac{e^2 \omega_{k \rightarrow i}^3}{\epsilon_0 c^3 h} \left| \int \Psi_k^* \cdot \vec{r} \cdot \Psi_i \cdot dr^3 \right|^2 \quad (12)$$

where $\omega_{k \rightarrow i} \approx 2B_0(j_i + 1)$ is the transition's angular frequency, \vec{r} is the charge displacement vector and $\Psi_{k/i}$ are the wavefunctions for states k and i respectively. For pure rotational transitions, eq. 12 simplifies to

$$A_{k \rightarrow i} = \frac{2}{3} \frac{\omega_{k \rightarrow i}^3}{\epsilon_0 h} \mu_0^2 \frac{j_k}{2j_k + 1} \quad (13)$$

where μ_0 is the permanent electric dipole moment of the molecule. Both the dipole values and the chosen rotational constants for the present anions were discussed earlier and given in the previous Section on the structural calculations.

Transition $j \leftarrow j'$	(C_5N^-)	(C_7N^-)
27 \leftarrow 28	7.26	1.12
28 \leftarrow 29	8.07	1.24
29 \leftarrow 30	8.94	1.38
30 \leftarrow 31	9.87	1.52
31 \leftarrow 32	10.9	1.67
32 \leftarrow 33	11.9	1.83
33 \leftarrow 34	13.0	2.01
34 \leftarrow 35	14.2	2.19
35 \leftarrow 36	15.5	2.38
36 \leftarrow 37	16.8	2.59
37 \leftarrow 38	18.2	2.81
38 \leftarrow 39	19.7	3.03
39 \leftarrow 40	21.3	3.28
40 \leftarrow 41	22.9	3.53

Table 1. Einstein Emission coefficients (A_{ij}) for C_5N^- and C_7N^- with $\Delta j = -1$. In units of 10^5 s^{-1} .

The results from the present calculations, which involve the same transitions as in the emission lines detected in the Interstellar medium by Cernicharo, J. et al. (2020); Cernicharo et al. (2023), are given by the data in Table 1.

The emission lines for the C_5N^- anion were observed in the IRC +10216 at an estimated temperature of (37 +/- 6) K. For the case of the C_7N^- anion the emission lines were observed in either the TMC-1 or the IRC +10216 CSEs at an estimated temperature of 26(+/-1.8) K. Given the very small spacing between the levels involved, if the two anions were to be considered under local thermal equilibrium, then the C_5N^- molecule would have its rotational states with j values from 25 and up to 35 with a fractional population around 25%. For the case of the C_7N^- anion, its rotational states with j values up to 41 would have a fractional population around 20%. We have therefore computed the rate coefficients involving that range of populated internal levels of the two title anions.

5. INELASTIC RATE COEFFICIENTS

Following the numerical evaluation of the relevant inelastic cross sections indicated in the previous Section, we further implemented the integration process of eq.(10) and employed the computed cross sections to generate inelastic rate coefficients over a range of about 50 K, the expected temperatures relevant to the CSE environments where detection of the present radical occurred, as discussed in our Introduction.

Examples for the case of the C_5N^- anion are displayed in the Figures reported in the following. Figure 4 shows excitation processes which start from the $j=25$ rotational state of this anion and end up in one

of the higher rotational states involved in the emission lines experimentally detected in (Cernicharo, J. et al. 2020). This example is meant to show how large the rates would be when considering excitation with fairly large Δj values beyond the more efficient cases with $\Delta j = +/-1$ discussed by our earlier work in (Biswas, R. et al. 2023).

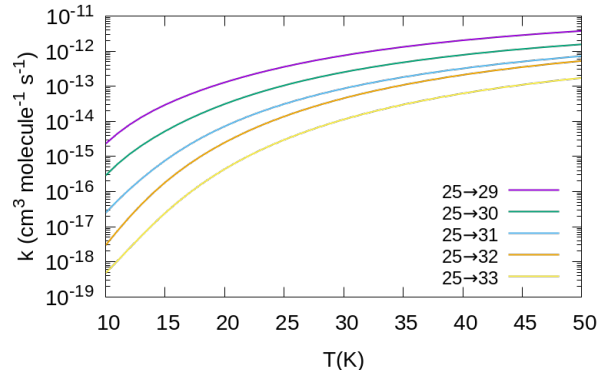


Figure 4. Computed excitation rate coefficients from the $j=25$ rotational state for the C_5N^- for transitions into the observed range of rotational states, over a temperature range of 50 K. See main text for further details.

Because the excitation processes shown in Fig. 4 involve large values of the Δj transition index, we can see that the corresponding rates have fairly small values at the lower temperatures and remain small up to the highest T values considered.

On the other hand, if we now consider the excitation processes shown by the data in Figure 5, we clearly see that the rate coefficients associated with the $\Delta j = +1$ value are much larger than the ones corresponding to the larger Δj reported in Figure 4. This is indeed to be expected from the changes in the relative energy gaps involved in the excitation processes, and as discussed in detail by us in our earlier work in ref (Biswas, R. et al. 2023). It follows from these findings that the efficient collisional re-populations of the levels in the observational emission lines of ref. Cernicharo, J. et al. (2020) would more easily occur from the contiguous levels that are active during those emission processes.

Looking at the data in Figure 5 which involve excitations associated with $\Delta j = +1$ transitions between the levels detected by the experimental work of Cernicharo, J. et al. (2020), we clearly see that all the rate coefficients are uniformly much larger than those associated with Δj values from +4 to +8 reported in Figure 4. These rates are therefore several orders of magnitude larger than those shown by Figure 4.

If we now turn to the de-excitation (collisional cooling) processes (presented in Figure 6), and involving

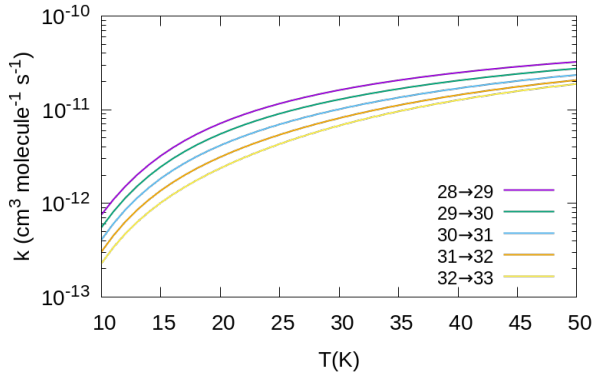


Figure 5. Computed excitation rate coefficients for $\Delta j=+1$ transitions over the observed range of rotational states for the C_5N^- . The data cover a temperature range up to 50 K. See main text for further details.

transitions with $\Delta j=-1$, we see that the rate coefficients are all of the order of $10^{-11} \text{ cm}^3 \text{ molecule}^{-1} \text{ s}^{-1}$, a size which makes them comparable with the corresponding excitation rates discussed in Figure 5. These will be the quantities that we shall further compare with the competing radiative processes, those driven by the large dipole moments of the present anions.

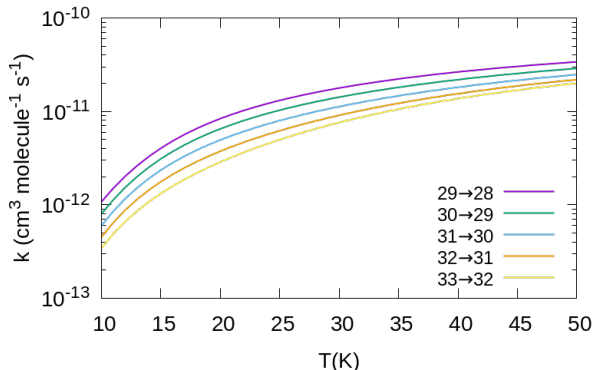


Figure 6. Computed de-excitation (cooling) rate coefficients from a variety of initial rotational states for C_5N^- the range of temperature values is up to 50 K. See main text for further details.

The set of calculations for the larger anionic chain, detected just recently by Cernicharo et al. (2023), and also involving excitation and de-excitation processes for the levels observed in their emission lines (see: Cernicharo et al. (2023)), are given in Figures 7 and 8.

The computed excitation rate coefficients are now nearly one order of magnitude larger than those pertaining to the shorter linear anion (see the previous Figure 5). Their range of values indicate how its smaller energy spacings shown by the Figure 3 are causing the corresponding excitation processes to be more efficient,

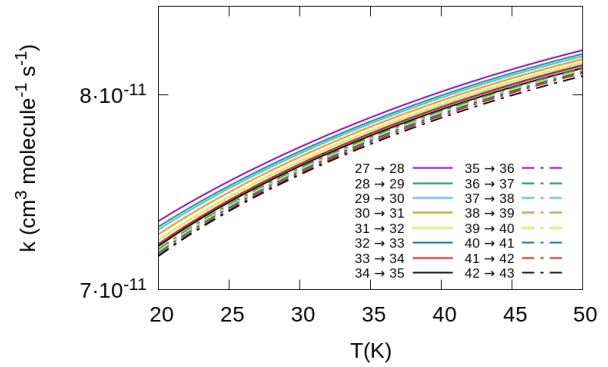


Figure 7. Computed excitation rate coefficients from a variety of initial rotational states for C_7N^- in collision with He atoms. The range of temperature values is up to 50 K. See main text for further details.

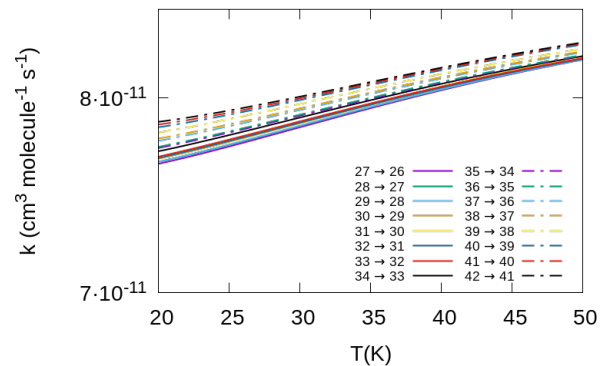


Figure 8. Computed de-excitation (cooling) rate coefficients from a variety of initial rotational states for C_7N^- in collision with He. The range of temperature values is up to 50 K. See main text for further details.

hence producing larger collision rate coefficients. A similar behaviour can also be gleaned by the results for the de-excitation (cooling) processes, reported in Figure 8. In this case, however, the differences with the results we had found for the C_5N^- at lower temperatures turn out to be smaller and therefore the two sets of de-excitation processes are very similar in size over the same range of temperatures.

It is interesting at this point to also compare the inelastic rate coefficients just obtained for the long chains discussed here with those which we have calculated in the past for smaller anions with larger energy spacing between rotational states: the C_2H^- and C_2N^- interacting with He atoms (Franz et al. 2020) and the CN^- interacting with He and H_2 partners: (González-Sánchez et al. 2020). In the case of the former anions, in fact, our earlier calculations of the excitation rate coefficients involving the lower rotational states (Franz et al. 2020) found such rates to be about one order of magnitude

larger than those reported here by Figures 5 and 7. Further, in the case of the CN^- anion, our earlier calculations in (González-Sánchez et al. 2020) also showed that the excitation rate coefficients were again about one order of magnitude larger than those reported here for the longer chains. Such findings suggest that the transitions involving the higher rotational states of the present study yield smaller rate coefficients than when the lower-lying rotational states are involved.

In the Introduction Section we have also pointed out that, besides He atoms, the simple hydrogen molecule is also one of the most abundant partner species within the environments where these anions have been observed. Hence, it is also useful to look at the collision-driven processes where the hydrogen molecule is the relevant partner. In our earlier work on the C_5N^- we have already considered excitation and de-excitation transitions induced by collision with the H_2 partner (Biswas, R. et al. 2023). Hence, the relevant collision processes among the experimentally detected levels are reported in Figure 9.

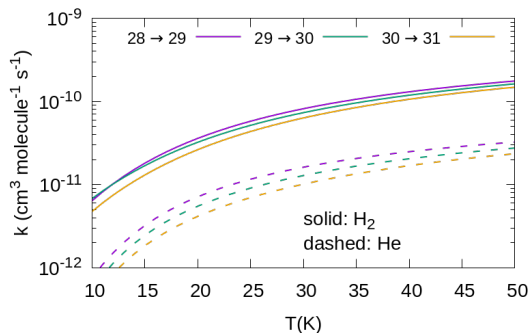


Figure 9. Comparing the computed collision-driven excitation processes into the higher rotational states of C_5N^- , for the He projectile and the $\text{H}_2(j=0)$ molecular partner. See main text for further details.

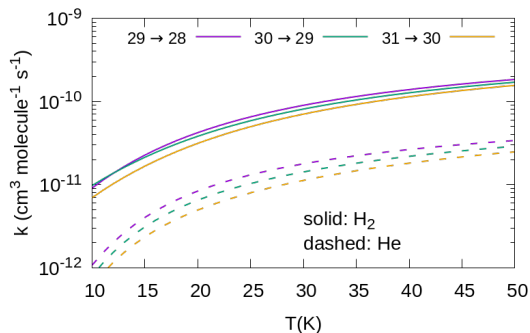


Figure 10. Same comparison of collision-driven transitions as in the previous Figure 9 but involving here the de-excitation processes in C_5N^- induced by both the He and the H_2 projectiles. See main text for further details.

We clearly see from the comparison reported by Figure 9 that the excitation rate coefficients from collisions with the $p\text{-H}_2$ molecule are much larger, by about one order of magnitude on average, than those obtained for the He projectile, thus indicating that both baryonic partners could substantially contribute to a possible, collision-driven, local thermal equilibration between the rotational levels of this target anion.

The de-excitation processes involving the $j=28, 29$ and 30 rotational states of the same anion, induced by collision with p -hydrogen molecules, are reported by Figure 10, where comparison is made with the same transitions induced by collision with He atoms. We see once more that such rates are now about one order of magnitude larger in comparison with those obtained for the He partner. Given the expected abundances of the H_2 molecule, we therefore also see that collision-driven population changes could be fairly significant for this partner, as they have already been shown to be important for the case of the He partner.

To acquire a more quantitative understanding of the size differences between the state-changing collision rate coefficients for the two types of partners with the C_5N^- anion, we report in Figures 11 and 12 the ratios between the two coefficient values for a sampling of three of the levels involved and over the relevant range of temperatures.

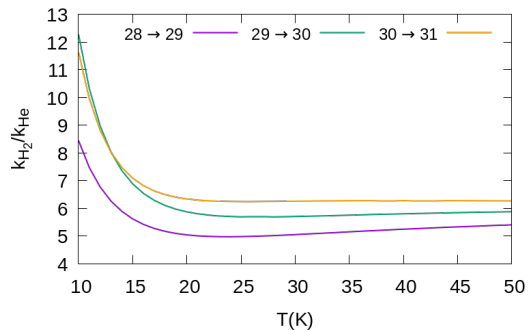


Figure 11. Computed numerical ratios between the two sets of rate coefficients discussed in this work for the C_5N^- anion in collision with H_2 and with He. The ratios involve, as examples, three of the relevant rotational states observed experimentally. They are given over a range of temperatures in line with that experimentally attributed to the relevant molecular clouds. See main text for further details.

It is clear from the data in those Figures that the rate coefficients pertaining to the H_2 projectile are uniformly larger than those obtained from the He partner: their dependence on T at the lowest temperatures above threshold peaks at factors of 10 and larger while becoming fairly constant in the range of T values between 15

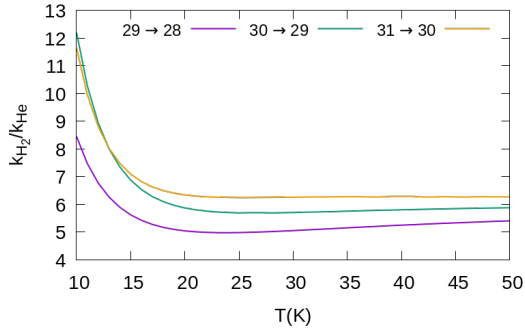


Figure 12. Same ratios as those discussed in Figure 11 but involving instead the de-excitation rate coefficients between the same rotational states. See main text for further details.

K and 50 K, covering the observed temperatures in the molecular clouds where the title anions have been recently detected: Cernicharo, J. et al. (2020); Cernicharo et al. (2023). This is an interesting result since, in the case of a linear anion of similar structure, e.g. for the C_7N^- discussed in this work, one could conceivably resort to scaling its present data just obtained for the He partner to estimate the rate coefficients needed for the H_2 . This option and its results will be further discussed in the following Section 6.

6. ANALYSIS OF CRITICAL DENSITIES

The assumption of a local thermodynamic equilibrium in different regions of the interstellar medium is expected, in general, to hold whenever the population of the excited levels under consideration is likely to be given by the Boltzman's law. In the present situation, this might happen whenever the rates of spontaneous emission from the internal levels of the polar anions are smaller than the rates of state-changing by collision with the most abundant partners present in that ISM region. This implies that the density in the interstellar gas for the partners should be significantly larger than some critical value so that the LTE assumption can be considered to be physically viable. The definition of a critical density (e.g. see: Lara-Moreno et al. (2019); Gianturco et al. (2021)) is given as follows:

$$n_{\text{crit}}^i(T) = \frac{A_{ij}}{\sum_{j \neq i} k_{ij}(T)} \quad (14)$$

where the critical density for any i^{th} rotational level is therefore obtained by giving equal weights to the consequences of either the collision-induced or the spontaneous emission processes. We have taken the rate coefficients discussed in Section 5, involving the rotational states which have been identified by the detection of our present anions, as discussed in the previous Section. We have also employed the computed spontaneous decay

Einstein coefficients discussed and presented in Section 4. It is also worth mentioning here that there is no sum over j values for the terms at the numerator since the dipole-driven contribution is by far the largest from any given initial i^{th} state.

Although the values of the particle densities is considered to vary widely in different ISM environments, so that several general models of the conditions in the molecular clouds suggest variations from the situation of the diffuse clouds (around 10^6 cm^{-3}) to dense clouds (around $10^{10} - 10^{12} \text{ cm}^{-3}$) as discussed, e.g., in (Snow & McCall 2006; Agúndez & Cernicharo 2006) and in the references reported there. On the other hand, the specific conditions in the molecular clouds where the present anions have been detected indicate that their densities are expected to be around $10^4 - 10^5 \text{ cm}^{-3}$. Hence, from our computed collision de-excitation rates of, say, Figure 9 for example, we can observe that the above values of expected particle densities can provide a specific range of collisional de-excitation efficiency in units of s^{-1} . Hence, in the present molecular clouds we obtain collision de-excitation quantities of the order of about 10^{-5} s^{-1} .

From the above considerations it follows that in such environments the collision-induced state-changing processes are faster than the spontaneous radiative emissions reported, for example, for the C_5N^- anion by our calculations in Table 1, while in the more diffuse environments the spontaneous decay channels could be comparable with the collision-induced ones.

The results in Figure 13 were obtained using the collision-induced rate coefficients calculated earlier by us for the C_5N^- partner (Biswas, R. et al. 2023). The fairly large values obtained for the critical densities are mainly controlled by the equally large spontaneous radiative emission coefficients, as reported in the present Table 1, which appear in the numerator of eq. (14).

A further example of the relative values of the critical densities for some of the rotational states which have been experimentally detected are reported in Figure 14, where we additionally present results obtained when molecular hydrogen is the collision partner of the C_5N^- anion, and compare them with those obtained for the He partner reported in Figure 13. As expected, the larger collision rate coefficients we had found for that molecular partner are now producing smaller values of the critical densities. Within the observed temperature range around 30 K we therefore see that both partners are likely to effectively compete with the radiative processes since the estimated critical densities shown by Figure 14 vary between 10^5 cm^{-3} and 10^6 cm^{-3} . Such range of values is well within the expected density values

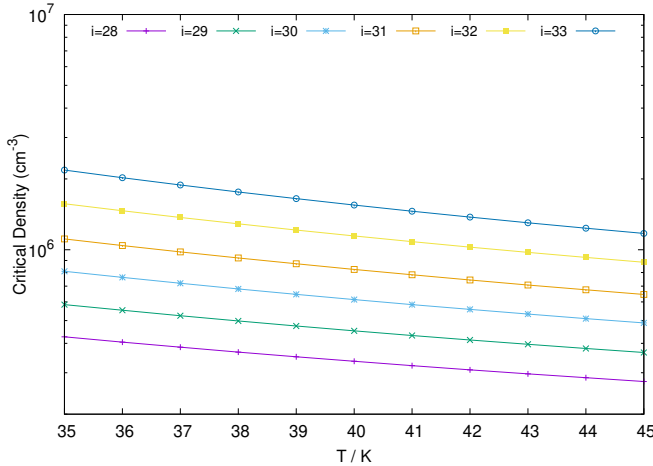


Figure 13. Computed critical densities for the C_5N^-/He system as obtained from Eq. (14), for temperatures from 35 K to 45 K. Present results are reported for the same rotational levels involved in the detection lines discussed in ref. (Cernicharo et al. 2023).

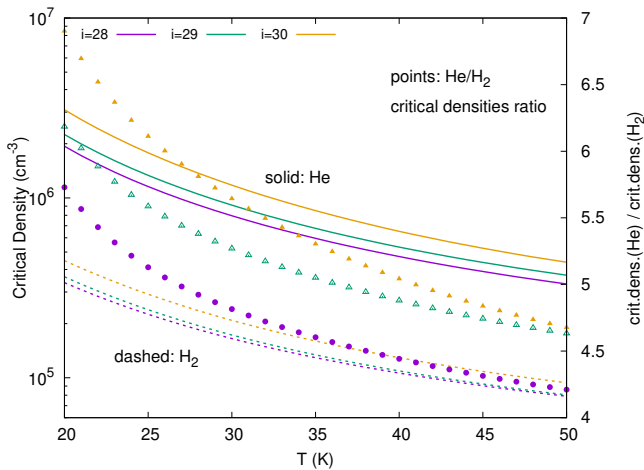


Figure 14. Comparison between the critical densities obtained for He as a collision partner (solid lines) and those pertaining the molecular hydrogen as the collision partner of the C_5N^- anion (dotted lines). The results are reported for some of the rotational levels involved in the detection lines of ref. (Cernicharo et al. 2023).

of the partner baryonic species in the interstellar environments where these anions have been detected. We have further extended the previous analysis of the critical densities to the next larger anion recently detected: the C_7N^- anion. In that case, we employ our accurate calculations of the collision rate coefficients obtained for He as a partner atom, while we generate by a scaling procedure those for the H_2 molecular partner. Hence, we use the He/ H_2 scaling factors we have obtained for the smaller C_5N^- anion and reported by Figures 11 and 12. That same ratio was thus applied to scale the data

for the longer chain anion in collision with He which we have been obtained in this work. The results of the exact and scaled rate coefficients obtained for the longer anion are given in Figures 15 and 16.

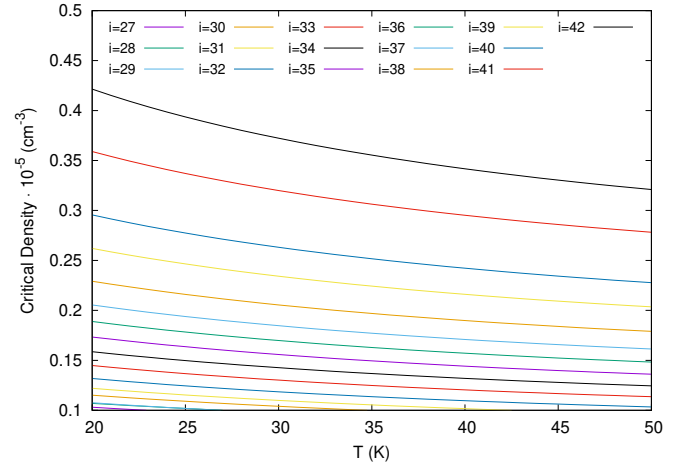


Figure 15. Computed critical densities for the C_7N^-/He system as obtained from Eq. (14), for temperatures from 20 K to 50 K, using the exact quantum rates discussed in the present paper. The results are reported for the same rotational levels involved in the detection lines discussed in ref. (Cernicharo et al. 2023).

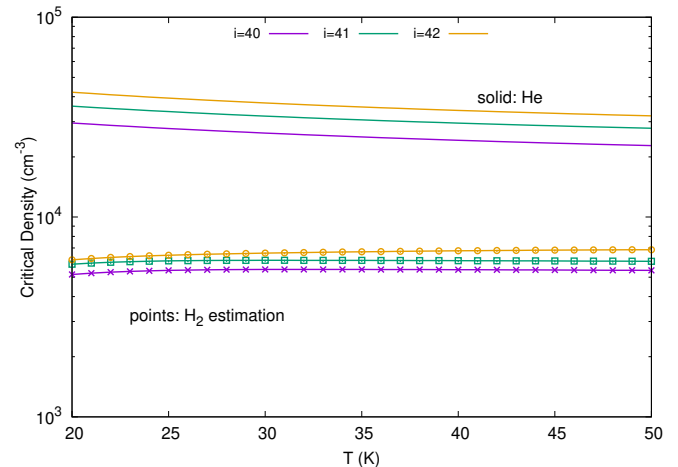


Figure 16. Comparison between the critical densities obtained for He as a collision partner (solid lines) and those pertaining the molecular hydrogen as the collision partner of the C_7N^- anion. The latter rates were obtained from the scaling procedure discussed in the main text. The results are reported for some of the rotational levels involved in the detection lines of ref. (Cernicharo et al. 2023).

We clearly see from the data in these two figures that the larger collision rate coefficients, exhibited by the longest cyanopolyne detected thus far, generate critical densities which are down to values around 10^4cm^{-3}

for the He partner and to around 10^3cm^{-3} for the H_2 molecular partner. Given the baryonic densities around 10^4cm^{-3} in the observational environments of these anions, our results suggest that the rotational state population of the C_7N^- anions exhibit critical density values which are large enough to allow the molecules to undergo collision-driven thermalization probabilities which are in competition with their radiative emission de-excitation paths. Under such conditions, therefore, to accurately know the collision-driven rate coefficients which we have computed would be important since their knowledge would allow us to establish whether the LTE approximation would be valid within their kinetic networks and whether it would provide reliable estimates of the relative populations reached under the densities of the CSEs where these anions are present. The knowledge of the actual collision rates with abundant partners like He (and H_2) is therefore relevant for more realistic modelings of the energy flow processes.

It is interesting to note here that in a recent work by Agúndez et al. (2023) excitation calculations were carried out using computed collision rate coefficients for a series of cyanopolyynes and polyynes. Their results indicate that the lines from anions accessible to radiotelescopes vary from being subthermally excited to being thermalized as the sizes of the anions increase and link the degree of non-LTE conditions on the H_2 volume densities and to the line frequencies. Since the present anions are the largest ones ever observed and not yet discussed in that work, we can argue from our present findings that the critical densities associated to the C_5N^- and the C_7N^- anions are well within the range of values indicated for the n- H_2 column densities that are suggested to vary between 1.0 and $7.5 \times 10^4\text{cm}^{-2}$. Hence, it stands to reason to assume that the rotational populations of these longer chains would be more likely to reach thermal conditions in the relevant molecular clouds.

7. PRESENT CONCLUSIONS

In the work reported in this paper we have analysed in some detail the behaviour of the excitation and de-excitation (cooling) rate coefficients associated with the rotational states of the two longest cyanopolyne chain anions, the C_5N^- and the C_7N^- , which have been detected so far in different CSE environments, as we have discussed in the Introduction section. The computed rate coefficients originate from the collisional interactions of these anions with He atoms and H_2 molecules, both species well known to be present in significant abundances in the same ISM environments. More specifically, the relative abundance of He with respect to H_2 is taken to be about 0.17 Agúndez et al. (2023) and usu-

ally considered to have about a 20% contribution to the state-changing probabilities in comparison with that of the neutral molecular partner. The abundance of the latter is considered to have a local density of the order of 10^4cm^{-3} Agúndez et al. (2023) and therefore relevant for its contribution to the rotational thermalization or sub-thermalization of the emission lines observed for the two title anions.

To further investigate the actual collision rate coefficients for both partners interacting with the two anionic chains, we have employed the accurate *ab initio* evaluation of both He and H_2 interactions with the C_5N^- already reported by us in our earlier work Biswas, R. et al. (2023). For the longer anionic chain of C_7N^- we have carried out new *ab initio* calculations of its interaction with He atoms and estimated those pertaining to the H_2 molecule by scaling the results for He with the same factors produced for the same partners in the case of C_5N^- . We have therefore been able to obtain realistic estimates of collision rate coefficients for both anions for the rotational states which had been found to be responsible of their emission lines recently observed in different CSE environments, as described in the Introduction Section.

Using the information we have on the energy spacing between the relevant rotational levels, and with the values we have computed for their permanent dipole moments, we have calculated the Einstein radiative coefficients acting in the cases of the observed emission lines. The combined use of such coefficients, and of the computed collision rate coefficients involving the same levels, has allowed us to obtain realistic estimates of the critical density values associated with both He and H_2 as partners of the title anions. We know, in fact, that the critical density (and thus the degree of departure from LTE) is very different depending on the dipole moment of the anion and on the frequency of the transition involved. In the present case we have specifically shown that the relevant emission lines which are at the detected temperatures of the cold clouds can be associated, in the case of the C_5N^- anion, with critical density values around 10^6cm^{-3} for the He partner at 35 K and around 10^5cm^{-3} for the H_2 partner at similar temperatures. The last quantity is indeed comparable with the expected baryonic density of the neutral molecular partner in the molecular clouds where these anions have been observed and therefore suggests that collisional thermalization can be very competitive with the radiative emission rates shown by this anion.

In the case of the next longer molecular cyanopolyne of our present calculations, we have further found larger collision rate coefficients but comparable radiative coef-

ficients, as shown by our data in Table 1. These findings have produced even smaller critical densities around the same temperatures discussed before: values between 10^4 and 10^5 cm^{-3} for the case of the He partner and scaled values for the H_2 partner of less than 10^4 cm^{-3} . These results further strengthen the suggestion that collision processes are definitely competitive with the radiative emission processes and can lead to final thermalization of the level populations of these anions in the observed ISM environments. Naturally, the quantities which we have computed in the present study are indeed very important to proceed with a more detailed analysis of the relevant kinetics since, in order to study the abundances and excitations of the present molecular anions in their interstellar sources we need to further know the physical parameters of the clouds, like the gas kinetic temperature and the H_2 volume density, but also the emission size of anions and the linewidth obtained from observation. In any event, our present, accurate calculations are already able to establish, from the obtained critical densities of both species at the observational temperatures, that collision events are indeed very competitive with the radiative efficiency indicated by their large dipole moment values and therefore that both long chains should be present with a thermal population of their rotational internal states.

8. ACKNOWLEDGEMENTS

One of us (L.G-S.) acknowledges the financial support by Ministerio de Ciencia e Innovación (Spain) MCIN/AEI/10.13039/501100011033 (Ref. PID2020-113147GA-I00 and PID2021-122839NB-I00). A.V. acknowledges Grant. No. EDU/1508/2020 (Junta de Castilla y León and European Social Fond). F.A.G. ac-

knowledges the support of the Computing Center of the Innsbruck University, where some of the present calculations were carried out. This research has also made use of the high performance computing resources of the Castilla y León Supercomputing Center (SCAYLE, www.scayle.es), financed by the European Regional Development Fund (ERDF). We are also grateful to Dr Marcelino Agúndez for several discussions and for providing us with a preprint of his recent work on ISM anions.

9. SUPPLEMENTARY MATERIAL

The following data have been prepared as Supplementary Material:

- (i) original raw points from the *ab initio* calculations,
- (ii) the multipolar coefficients for the Legendre expansion of the rigid rotor potential for the $\text{C}_7\text{N}^-/\text{He}$ system,
- (iii) the computed inelastic cross sections,
- (iv) the corresponding rate coefficients obtained from the 2D-RR-PES employed in this work for the C_7N^- anion;
- (v) The critical density values obtained for both anions and linked to their collision data for either He or H_2 are all provided as Supplementary Material.

All the above data are available at GREDOS:

[10.14201/gredos.153158](https://doi.org/10.14201/gredos.153158)

10. DATA AVAILABILITY

The data that support the findings of this study are available within the article and in its supplementary material, their accessibility is described via the link reported in the previous Section.

REFERENCES

- Agúndez, M., & Cernicharo, J. 2006, *ApJ*, 650, 374, doi: [10.1086/506313](https://doi.org/10.1086/506313)
- Agúndez, M., Marcelino, N., Tercero, B., Jiménez-Serra, I., & Cernicharo, J. 2023, *A&A*, arXiv:2307.04487v1
- Agúndez, M., Cernicharo, J., Guélin, M., et al. 2008, *A&A*, 478, L19, doi: [10.1051/0004-6361/20078985](https://doi.org/10.1051/0004-6361/20078985)
- Agúndez, M., Cernicharo, J., Guélin, M., et al. 2010, *A&A*, 517, L2, doi: [10.1051/0004-6361/201015186](https://doi.org/10.1051/0004-6361/201015186)
- Arthurs, A. M., & Dalgarno, A. 1960, *Proc. R. Soc. A*, 256, 540, doi: [10.1098/rspa.1960.0125](https://doi.org/10.1098/rspa.1960.0125)
- Biswas, R., Giri, K., González-Sánchez, L., et al. 2023, *MNRAS*, 522, 5775, doi: doi.org/10.1093/mnras/stad1261
- Botschwina, P., & Oswald, R. 2008, *Journal of Chemical Physics*, 129, 044305, doi: [10.1063/1.2949093](https://doi.org/10.1063/1.2949093)
- Brown, J. M., & Carrington, A. 2003, *Rotational Spectroscopy of Diatomic Molecules* (Cambridge: Cambridge University Press)
- Brünken, S., Gupta, H., Gottlieb, C., McCarthy, M., & Thaddeus, P. 2007, *The Astrophysical Journal*, 664, L43, doi: [10.1086/520703](https://doi.org/10.1086/520703)
- Cernicharo, J., Guélin, M., Agúndez, M., McCarthy, M. C., & Thaddeus, P. 2008, *The Astrophysical Journal*, 688, L83–L86, doi: [10.1086/593183](https://doi.org/10.1086/593183)
- Cernicharo, J., Pardo, J., Cabezas, C., et al. 2023, *A&A*, 670, L19, doi: doi.org/10.1051/0004-6361/202245816

- Cernicharo, J., Guélin, M., Agúndez, M., et al. 2007, *A&A*, 467, L37, doi: [10.1051/0004-6361:20077415](https://doi.org/10.1051/0004-6361:20077415)
- Cernicharo, J., Marcelino, N., Pardo, J. R., et al. 2020, *A&A*, 641, L9, doi: [10.1051/0004-6361/202039231](https://doi.org/10.1051/0004-6361/202039231)
- Deega, M. J. O., & Knowles, P. J. 1994, *Chem. Phys. Lett.*, 227, 321
- Dunning Jr, T. H. 1989, *J. Chem. Phys.*, 90, 1007
- Faure, A., Szalewicz, K., & Wiesenfeld, L. 2011, *The Journal of chemical physics*, 135, doi: [10.1063/1.3607966](https://doi.org/10.1063/1.3607966)
- Franz, J., González-Sánchez, L., Mant, B. P., Wester, R., & Gianturco, F. A. 2020, *J.Chem.Phys.*, 152, 234303
- Frisch, M. J., Trucks, G. W. and Schlegel, H. B., Scuseria, G. E., et al. 2009, Gaussian, Inc; Wallingford,CT,USA
- Gianturco, F. 1979, *Lect. Notes Chem.*, Springer Verlag, Berlin
- Gianturco, F. A., Giri, K., González-Sánchez, L., et al. 2021, *J. Chem. Phys.*, 154, 054311, doi: [10.1063/5.0040018](https://doi.org/10.1063/5.0040018)
- González-Sánchez, L., Mant, B. P., Wester, R., & Gianturco, F. A. 2020, *Ap. J.*, 75, 897
- Hutson, J. M., & Sueur, C. R. L. 2019a, *Computer Physics Communications*, 241, 9, doi: [10.1016/j.cpc.2019.02.014](https://doi.org/10.1016/j.cpc.2019.02.014)
- . 2019b, MOLSCAT a program for non-reactive quantum scattering calculation on atomic and molecular collisions. <https://github.com/molscat/molscat>
- Jerosimić, S. V., Gianturco, F. A., & Wester, R. 2018, *Phys. Chem. Chem. Phys.*, 20, 5490, doi: [10.1039/C7CP05573K](https://doi.org/10.1039/C7CP05573K)
- Khadri, F., Chefai, A., & Hammami, K. 2020, *Monthly Notices of the Royal Astronomical Society*, 498, 5159, doi: [10.1093/mnras/staa2746](https://doi.org/10.1093/mnras/staa2746)
- Khamesian, M., Douguet, N., Fonseca dos Santos, S., et al. 2016, *Phys. Rev. Lett.*, 117, 123001, doi: [10.1103/PhysRevLett.117.123001](https://doi.org/10.1103/PhysRevLett.117.123001)
- Kouri, D., & Hoffman, D. 1997, Truhlar D.G., Simon B. (eds) *Multiparticle Quantum Scattering With Applications to Nuclear, Atomic and Molecular Physics*, 89, Springer, New York, NY, doi: <https://doi.org/10.1007/978-1-4612-1870>
- Lara-Moreno, M., Stoecklin, T., & Halvick, P. 2019, *MNRAS*, 486, 414
- López-Durán, D., Bodo, E., & Gianturco, F. A. 2008, *Comput. Phys. Commun.*, 179, 821
- Martinazzo, R., Bodo, E., & Gianturco, F. A. 2003, *Comput. Phys. Commun.*, 151, 187
- Massó, H., & Wiesenfeld, L. 2014, *The Journal of Chemical Physics*, 141, doi: [10.1063/1.4900856](https://doi.org/10.1063/1.4900856)
- McCarthy, M. C., Gottlieb, C. A., Gupta, H., & Thaddeus, P. 2006, *The Astrophysical Journal*, 652, L141, doi: [10.1086/510238](https://doi.org/10.1086/510238)
- Remijan, A., Scolati, H., Burkhardt, A., et al. 2023, *ApJL*, 944, L45, doi: doi.org/10.3847/2041-8213/acb648
- Remijan, A. J., Hollis, J. M., Lovas, F. J., et al. 2007, *The Astrophysical Journal*, 664, L47, doi: <https://doi.org/10.1086/520704>
- Sahnoun, E., Wiesenfeld, L., Hammami, K., & Jaidane, N. 2018, *The Journal of Physical Chemistry A*, 122, 3004, doi: [10.1021/acs.jpca.8b00150](https://doi.org/10.1021/acs.jpca.8b00150)
- Satta, M., Gianturco, F. A., Carelli, F., & Wester, R. 2015, *ApJ*, 799, 228, doi: [10.1088/0004-637X/799/2/228](https://doi.org/10.1088/0004-637X/799/2/228)
- Secrest, D. 1979, Bernstein R.B. (eds) *Atom - Molecule Collision Theory*, Plenum, New York, doi: <https://doi.org/10.1007/978-1-4613-2913-8>
- Snow, T. P., & McCall, B. J. 2006, *Annu.Rev. Astronom. Astrophys.*, 44, 367, doi: [10.1146/annurev.astro.43.072103.150624](https://doi.org/10.1146/annurev.astro.43.072103.150624)
- Thaddeus, P., Gottlieb, C. A., Gupta, H., et al. 2008, *The Astrophysical Journal*, 677, 1132, doi: [10.1086/528947](https://doi.org/10.1086/528947)
- Weigend, F., & Ahlrichs, R. 2005, *Phys.Chem. Chem. Phys.*, 7, 3297
- Woon, D. E., & Dunning Jr, T. H. 1994, *J. Chem. Phys.*, 100, 2975